SO_x Storage Materials under Lean−Rich Cycling Conditions. Part I: Identification of Transient Species

Hendrik Dathe, Peter Haider, Andreas Jentys, and Johannes A. Lercher*

Department of Chemistry, Technische Universität München, Lichtenbergstr. 4, D-85747 Garching, Germany

Received: February 24, 2006; In Final Form: April 6, 2006

The SO_x uptake of second generation sulfur trapping materials was studied by in situ IR spectroscopy under lean−rich cycling conditions. The combination of advanced chemometric methods including generalized 2D correlation analysis, 2D sample−sample correlation analysis, and multivariate curve resolution with alternating least squares allowed the detection of the species involved in the storage process. The formation of the bulk sulfate species was always accompanied by the consumption of carbonates. The reduction of a transient surface sulfate species was identified as the key parameter in the storage process under dynamic conditions. Three distinct reaction regimes were differentiated on the industrial materials under SO_x trapping conditions being imperceptible from conventional spectra.

Introduction

Tighter legislation restrictions for the emissions from mobile sources (EURO IV) require new techniques for NO_x removal from lean-burn engine exhausts. In this context, the NO_x storage-reduction concept (NSR), based on a cycling operation mode of the engine is probably currently the most promising concept.[1−3] In this process, the NO_x species formed are trapped on the catalyst surface during an extended period of low fuel consumption in oxygen excess (lean mode). The reduction occurs during a short period in reducing atmosphere, that is, under fuel-rich conditions (rich mode). Unburned hydrocarbons in addition to CO are used to reduce the NO_x species. However, the NSR catalysts are severely deactivated by the presence of SO_2 in the exhaust gas stream, which adsorbs irreversibly on the catalyst surface and leads to the blockage of the NO_x sorption sites by the formation of thermodynamically favored sulfate species.[3−5]

An approach to overcome this limitation is the implementation of a SO_x trap before the NSR catalyst to remove the sulfur species present in the exhaust gas stream. Several S-trapping materials are available, containing a refractory support (e.g., Al_2O_3, CeO_2, ZrO_2), an oxidation component (e.g., Pt, Rh, and Mn), and a sulfur storage component (e.g., Mg, Na, Ca, and Ba).[6−8] Apart from a high sulfur storage capacity, the stability of the sulfur species under fuel-rich reaction conditions is an essential feature of S-trap materials to avoid the release of SO_x in the regeneration cycles of the NSR catalyst.[9,10] Consequently, for further improvement of the performance of these materials, understanding the dynamic SO_2 storage processes under lean−rich cycling operation conditions is essential.

The application of in situ IR spectroscopy to study the formation of sulfate species on metal oxides is widely explored.[3,11−13] The major hindrances in investigating industrial mixed metal oxides under in situ conditions are the strongly overlapping spectral regions of the sulfates formed and the absorption of carbonates present in the materials that mask subtle spectral features. Generalized 2D correlation analysis, however, can significantly help to resolve such subtle changes.[14−18] Moreover, a detailed investigation of the periodical behavior of the spectral intensities of interest can be performed by the 2D sample−sample correlation analysis introduced by Sasic et al., which can reveal the concentration dynamics in a spectral system through tracking spectral changes at all wavenumber points of interest.[19,20] In combination with other chemometric methods, the 2D correlation analysis can even reveal temporary effects in a dataset, for example, with the concept of fixed-size moving window evolving factor analysis (FSMWEFA) applied to the 2D correlation analysis.[21,22] Besides the identification of the spectral regimes influenced by a (concentration) perturbation, the determination of the spectra of the pure components by applying the factor analysis is important for a detailed understanding.[23−26]

In the present paper, we address methods to identify the nature of sulfur species formed on an industrial SO_x sorbent material using time-resolved in situ IR spectroscopy at typical diesel exhaust gas conditions. The combination of advanced chemometric methods is used to analyze the datasets to reveal the nature and the dynamic variations of surface and bulk species being present.

Experimental Section

Material. A Cogel $CuO-Al_2O_3$ was synthesized by a proprietary procedure of Venezia Tecnologia and calcined in air at 823 K for 3 h. The support was further impregnated with Ba and calcined again in air at 823 K for 1 h leading to the final material ($Ba/CuO-Al_2O_3$).

In Situ IR Spectroscopic Experiments. IR spectroscopic experiments were carried out in a flow cell in the transmission-absorption mode using a Perkin-Elmer 2000 − FTIR spectrometer. For the measurements, the samples were pressed into self-supporting wafers. The gas compositions of the mixtures under lean and rich conditions are shown in Table 1. All experiments were carried out at 523 K. The cycling times were typically set to 240 s for lean operation mode and 18 s for rich operation mode. Prior the lean−rich cycling operation, the catalyst was pretreated under lean conditions for 2 h.

* Technische Universität München, Lichtenbergstr. 4, D-85747 Garching, Germany. Tel.: +49 89 289 13540. Fax.: +49 89 289 13544. E-mail: Johannes.lercher@ch.tum.de.

10.1021/jp0611931 CCC: $33.50
Published on Web 05/17/2006

TABLE 1: Typical Gas Composition Applied during in Situ IR Spectroscopic Experiments

gas	lean operation	rich operation
O_2	12%	4%
CO_2	4%	8.5%
SO_2	10 ppm	10 ppm
NO_2	30 ppm	50 ppm
C_3H_6	0%	0.5%
H_2	0%	1%
He	balance to 200 mL/min	balance to 200 mL/min

Mathematical Methods. All calculations were performed using Matlab 6.5. The number of principle components was selected using the program developed by Malinowski.[25] All calculations involving Multivariate curve resolution with alternating least squares (MCR-ALS) were performed using the Matlab programs developed by Tauler et al.[27] Prior to the calculations a background correction was performed using the concept by Mazet et al.[28] A moving window approach involving five consecutive spectra was used as dataset. Hence, the dataset covers either spectra solely recorded under lean operation mode or spectra recorded under lean and rich operation mode.

2D Correlation Analysis. The 2D correlation analysis was performed following the method described by Noda et al.[16,29] as shown in eq 1.

$$\Phi(\nu_1, \nu_2) = \frac{1}{n-1}\cdot DD^T \quad \Psi(\nu_1, \nu_2) = \frac{1}{n-1}\cdot DND^T$$
$$\text{with } N_{jk} = \begin{cases} 0 & \text{for } j=k \\ \dfrac{1}{\pi\cdot(k-j)} & \text{for } j\neq k \end{cases} \quad (1)$$

Each column of the data matrix D represents a spectrum, which was mean centered prior to the calculation. The synchronous 2D correlation intensity $\Phi(\nu_1, \nu_2)$ is regarded as the covariance between the intensities at the spectral frequencies ν_1 and ν_2 of the two series of spectra measured as function of time. Autocorrelation peaks located on the diagonal line corresponding to $\nu_1 = \nu_2$ for $\Phi(\nu_1, \nu_2)$ are always positive (note that this is not necessarily true for heterospectral analysis) and form a square with two symmetric cross-peaks at the corresponding intersections.[16] The sign of the cross-peaks indicates whether the changes are directly or reversibly (indirectly) correlated, that is, if the changes in intensity occur in the same (positive sign) or in different directions (negative sign). The asynchronous correlation intensity $\psi(\nu_1, \nu_2)$ represents sequential or successive changes in the series of time-resolved spectra.[16] Because of the oscillating nature of the bands as an effect of the lean−rich modulation of the gas mixture, the asynchronous technique is not utilized because artifacts may appear under these circumstances.[30,31]

The 2D sample−sample correlation analysis was performed applying eq 2. With this technique, a detailed investigation of the periodical behavior of the spectral intensities of interest was performed following the concentration profiles directly. The cross-product matrix $\Phi_1(\nu_1, \nu_2)$ represents the correlations between the different *spectra* of dataset D, while the wavenumber−wavenumber 2D correlation analysis $\Phi(\nu_1, \nu_2)$ shows the relation among the *spectral variables*, for example, wavenumbers.[18]

$$\Phi_1(\nu_1,\nu_2) = \frac{1}{n-1}\cdot D^T D \quad (2)$$

The factor analysis is based on the hypothesis that an original data matrix can be reconstructed from a linear combination of a limited number of significant loading vectors and scores. The raw data matrix consists of r spectra with c data points. Here, every row of the data matrix corresponds to one spectrum being a linear combination of the spectra of the pure components as shown in eq 3.

$$A_{\mathrm{rc,raw}} = C_{\mathrm{m,abstract}}\cdot S^T_{\mathrm{nc,abstract}} + E_{\mathrm{rc}} = A_{\mathrm{rc,PCA}} + E_{\mathrm{rc}} \quad (3)$$

A critical point in every factor analysis is the determination of the number of essential components n present in the dataset. The following (statistical) tests were used to unambiguously determine the number of factors in the dataset: reduced eigenvalue (REV), reduced eigenvalue ratio (REVR), variance and cumulative variance of each eigenvalue, F-test and the corresponding significance level, and the real error (RE) of the remaining factors.[25] Afterward, the related coefficient or concentration matrix C and the spectra matrix S can be calculated. However, the coefficient matrix C and the matrix of the pure components, S^T, are only the so-called abstract matrices leading to a mathematically correct, but possibly physically meaningless, result.[23,24,26,32−34] To obtain "real" or physically meaningful coefficients and spectra matrices the "abstract" solutions have to be transformed with the transformation matrix T (rotational ambiguity) as shown in eq 4.[26,33,34] The obtained matrices C_{real} and S_{real} are subject to the so-called intensity ambiguity as shown in eq 5

$$A_{(\mathrm{rxc})} = C_{\mathrm{rxct}}\cdot S^T_{\mathrm{nxr}} = C_{\mathrm{abstr}}\cdot S^T_{\mathrm{abstr}}$$
$$A = C_{\mathrm{abstr}}\cdot S^T_{\mathrm{abstr}} = C_{\mathrm{abstr}}(T\cdot T^{-1})\cdot S^T_{\mathrm{abstr}}$$
$$A = (C_{\mathrm{abstr}}\cdot T)\cdot(T^{-1}\cdot S^T_{\mathrm{abstr}})$$
$$A = C_{\mathrm{real}}\cdot S_{\mathrm{real}} \quad (4)$$
$$A = \sum_{j=1}^{n}\left[\left(\frac{1}{k_j}\cdot\vec{c}_j\right)\cdot(k_j\cdot\vec{s}_j^{\,T})\right] \quad (5)$$

with k_j being n scalars.[26] The application of certain constraints to solve the equations above is indispensable; possible constraints are nonnegative for the spectra and the coefficient profiles.

For dealing with the rotational ambiguity, the multivariate curve resolution with alternating least-squares (MCR-ALS) concept was used.[35] In the first step, S^T is calculated from an initial estimation for the coefficient profile. In each iteration step S^T and C can then be calculated by the following approach (see eqs 6 and 7):[24,36]

$$A^* = C\cdot S^T$$
$$C^T\cdot A^* = C^T\cdot C\cdot S^T$$
$$(C^TC)^{-1}\cdot C^T\cdot A^* = (C^TC)^{-1}\cdot C^TC\cdot S^T$$
$$S^T = (C^TC)^{-1}\cdot C^T\cdot A^* \quad (6)$$
$$C = A^*\cdot S\cdot(S^TS)^{-1} \quad (7)$$

Results

Adsorption of NO_2 under Lean−Rich Conditions. The time-resolved IR spectra during adsorption of NO_2 on the Ba/CuO−Al_2O_3 sample at 523 K under lean operation conditions applying a SO_2 free gas mixture (Table 1) are shown in Figure

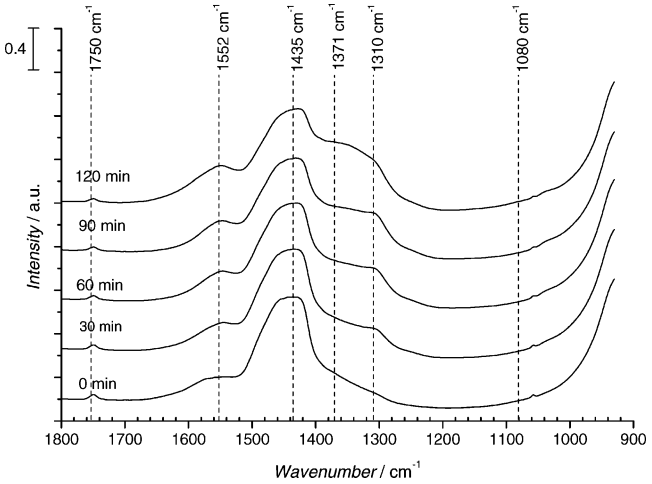

Figure 1. Time-resolved in situ IR spectra of $Ba/CuO-Al_2O_3$ under lean conditions at the mixture shown in Table 1 in the absence of SO_2 at 573 K.

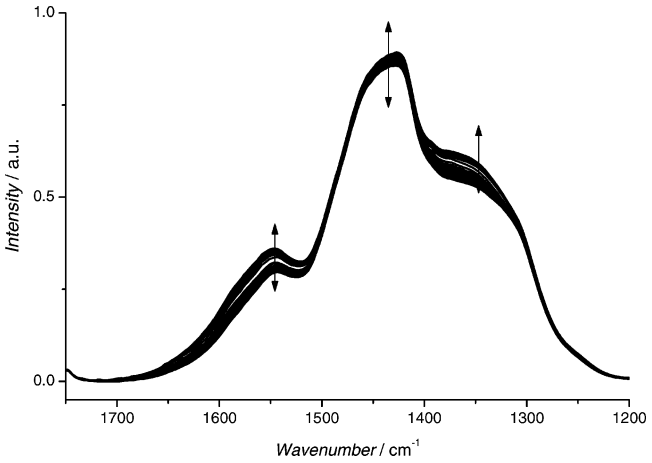

Figure 2. Time-resolved in situ IR spectra of $Ba/CuO-Al_2O_3$ under lean−rich conditions (240 s lean, 72 s rich) in the absence of SO_2 Δt = 30 min.

1. For the fresh material the bands at 1750, 1557, and 1437 cm^{-1} are attributed to carbonate species.[13,37] During the first 30 min of NO_2 exposure a band is formed at 1310 cm^{-1}, which can be assigned to nitrato/nitro species located on Cu^+.[38,39] With increasing NO_2 exposure the formation of bands located at 1552 cm^{-1} ($Cu^{2+}\langle{}^{O}_{O}\rangle$ N−O), 1435 cm^{-1} ($Ba-N\langle{}^{O}_{O}\rangle$, 1371 cm^{-1}($Cu^{2+}(NO_3^-)_2$), and a small band around 1080 cm^{-1} (Al−O−N−O) indicate the formation of nitrates on all cationic sites present.[3,40−42] In principle, the formation of nitrates on other sites cannot be excluded because the strong carbonate band could mask spectral contributions from such adsorption sites.

After 2 h time on stream under lean reaction conditions the intensities of the bands did not increase further. Under lean−rich cycling reaction conditions the bands at 1552, 1435, 1371, and 1080 cm^{-1} were affected (see Figure 2). However, the determination of the surface concentration of these species as function of the cycling time (e.g., by spectral subtraction) was not attempted because of the dominating contribution of the carbonate bands. It is important to note that the characteristic vibration of $C_3H_7-NO_2$ and an organic nitrito compound (C_3H_7-ONO), typically also involved in the SCR reaction pathway, also show bands in this wavenumber range as presented in the literature.[40,43,44]

For tracking spectral changes of the nitrate and carbonate species a 2D sample−sample correlation analysis was performed from 1650 to 1300 cm^{-1}, including all spectral features identified from the 1D plot. Figure 3 depicts the 2D sample−sample correlation analysis during NO_2 exposure between t = 120 and 150 min.

The changes in the spectral intensity occurring in the wavenumber region selected can be followed along the diagonal of Figure 3 (left) and are plotted in Figure 3 (right) to allow a more thorough investigation of the time dependence of the surface concentration changes. Five well-resolved maxima are found at around 125, 130, 135, 140, and 145 min, while rich conditions are applied, which is assigned to an overall intensity increase. After the gas mixture is switched to lean operation mode, the intensity of these features starts to level off. This leads to the conclusion that the three peaks located in this region (1371, 1435, and 1552 cm^{-1}; see Figure 1) increase during the rich mode and decrease during the lean mode. Note that in this spectral region carbonate and NO_x species appear; therefore, a combination of the two regimes are observed, which involves the reduction of the carbonate species and the adsorption of NO_x species formed under lean conditions.

The 2D sample−sample correlation analysis was repeated (not shown here) with datasets consisting of only one of the three peaks (i.e., the datasets were shortened leading to ranges from 1600 to 1500 cm^{-1}, 1500 to 1400 cm^{-1}, and 1400 to 1300 cm^{-1}), which leads to identical results. Moreover, it was found that the same pattern was obtained if the wavenumber region was set from 1000 to 1200 cm^{-1} (Al−O−N−O, see Figure 1) although the pattern was less intense in this region (graphs not

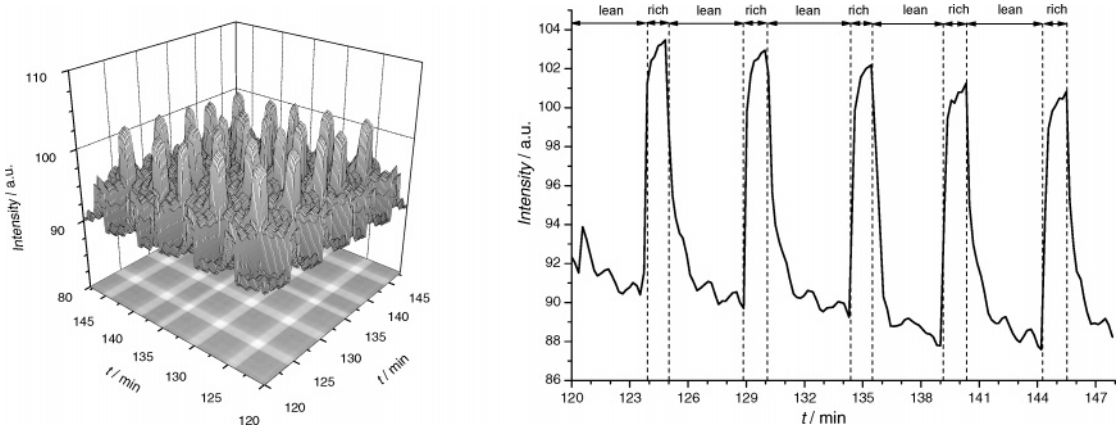

Figure 3. 2D sample−sample correlation analysis calculated for the dataset shown in Figure 2 for five lean−rich cycles (left) 3D surface plot, (right) corresponding diagonal.

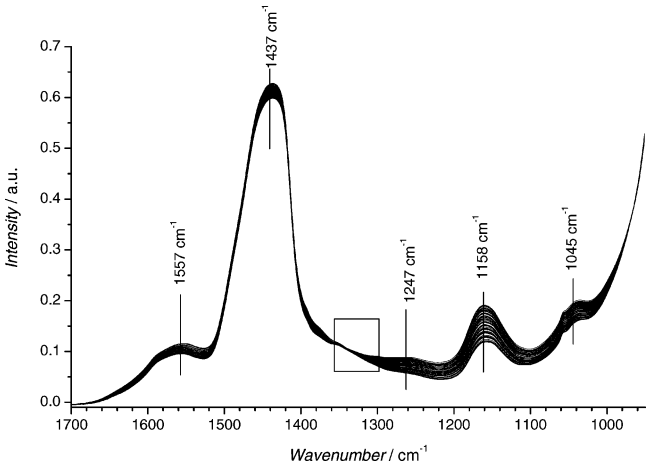

Figure 4. Time-resolved in situ IR spectra obtained for the Ba/CuO−Al_2O_3 recorded under lean−rich cycling conditions (see Table 1) at 523 K.

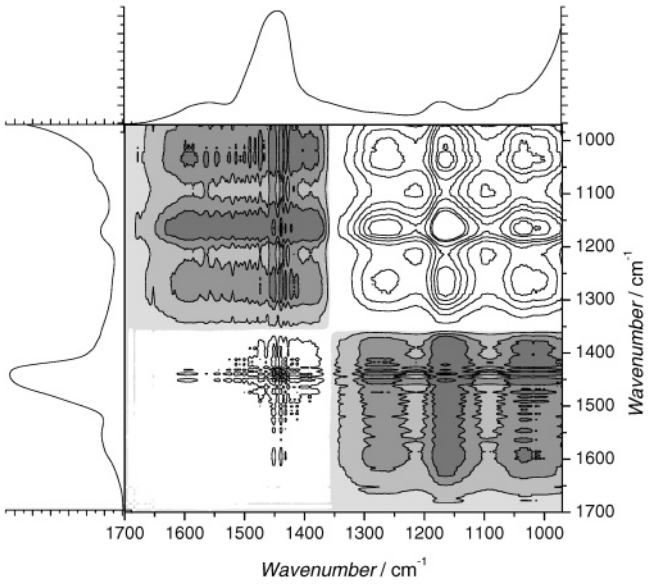

Figure 5. Synchronous correlation contour plots calculated by means of moving window correlation analysis from a dataset consisting of five spectra recorded under lean conditions at 523 K on Ba/CuO−Al_2O_3.

shown here). Similar experiments carried out at various reducing times also showed the same trend.

SO_2 Adsorption during Lean−Rich Cycling Conditions. In situ IR spectra recorded during lean−rich cycling with a time for lean conditions of 240 s and for rich conditions of 18 s after 2 h in lean conditions are shown in Figure 4. The bands observed at 1247, 1158, and 1045 cm^{-1} indicate the presence of surface and bulk sulfates.[5,12,39,45−48] Nevertheless, because of the strongly overlapping bands of the various sulfates an unequivocal assignment was not possible. It is also important to note that the region between 1350 and 1290 cm^{-1} was affected by the lean−rich cycling, but a clear maximum was not observed.

For the entire dataset an overall increase in the intensity of the bands assigned to sulfur species was observed under lean conditions (see Figure 4). Similar to the SO_2 free experiment, however, the spectral changes during switching between lean−rich could not be followed directly. One complete lean−rich cycle consists of nine consecutive spectra (∼29 s per spectra). When applying 18 s for reducing conditions (typical reducing time in diesel engines), at least one spectrum contains information about the fuel-lean and the fuel-rich situation due to the experimental constraints.

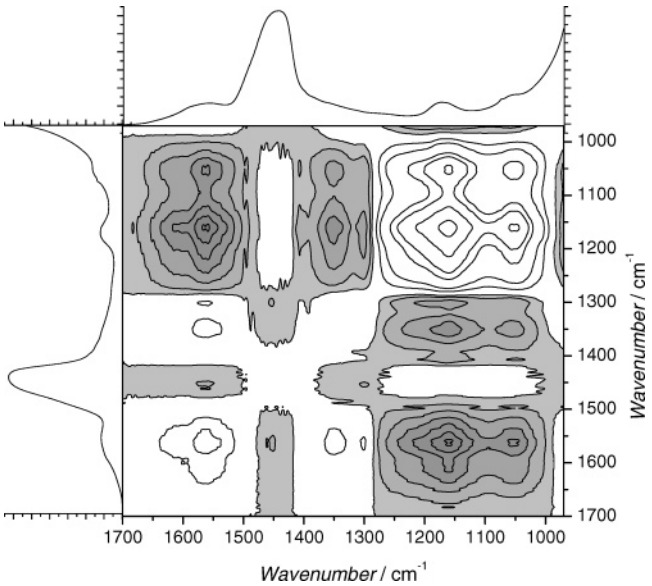

Figure 6. Synchronous correlation plots calculated by means of moving window correlation analysis from a dataset (Figure 4) consisting of five spectra recorded (four under lean and one rich conditions) at 523 K on Ba/CuO−Al_2O_3.

TABLE 2: Peak Positions and Peak Signs Determined for the Synchronous 2D Correlation Plots Including Spectra Recorded in the Lean Mode

location	peak sign	direction of change
1158−1045 cm^{-1}	positive	increasing
1158−1295 cm^{-1}	positive	increasing
1158−1350 cm^{-1}	positive	increasing
1158−1442 cm^{-1}	negative	decreasing
1158−1557 cm^{-1}	negative	decreasing

TABLE 3: Peak Positions and Peak Signs Determined for the Synchronous 2D Correlation Plots Including Spectra Recorded in the Rich Mode for Ba/CuO−Al_2O_3 at 523 K

location	peak sign	direction of change
1158−1045 cm^{-1}	positive	increasing
1158−1295 cm^{-1}	negative	decreasing
1158−1350 cm^{-1}	negative	decreasing
1158−1442 cm^{-1}	positive	increasing
1158−1557 cm^{-1}	negative	decreasing

To overcome this limitation the dataset was analyzed by the moving window 2D correlation analysis. The synchronous plot calculated from five spectra recorded under lean operation mode is depicted in Figure 5. Three well-defined auto-peaks appear at the diagonal at the locations 1247, 1158, and 1045 cm^{-1}. The positions as well as the signs of the cross-peaks indicating the correlation of the spectral changes at the respective positions are compiled in Table 2. The variation at the peak centered at 1247 cm^{-1} is shown by large distinct positive cross-peaks located at the intersections Φ(1247 cm^{-1}, 1158 cm^{-1}) and Φ-(1247 cm^{-1}, 1045 cm^{-1}) reveal a synchronous increase of these IR bands. The bands at 1247, 1158, and 1045 cm^{-1} can be assigned to various sulfate species representing the sulfate formation as shown above.[13,49] The small negative peaks observed at the intersection of the IR band centered at 1442 cm^{-1} (carbonate species) with the IR bands is assigned to sulfate species and indicates the replacement of carbonates, while sulfates formed under lean conditions.

Figure 6 shows the synchronous plot obtained from five consecutive spectra, four spectra recorded under lean and one spec-

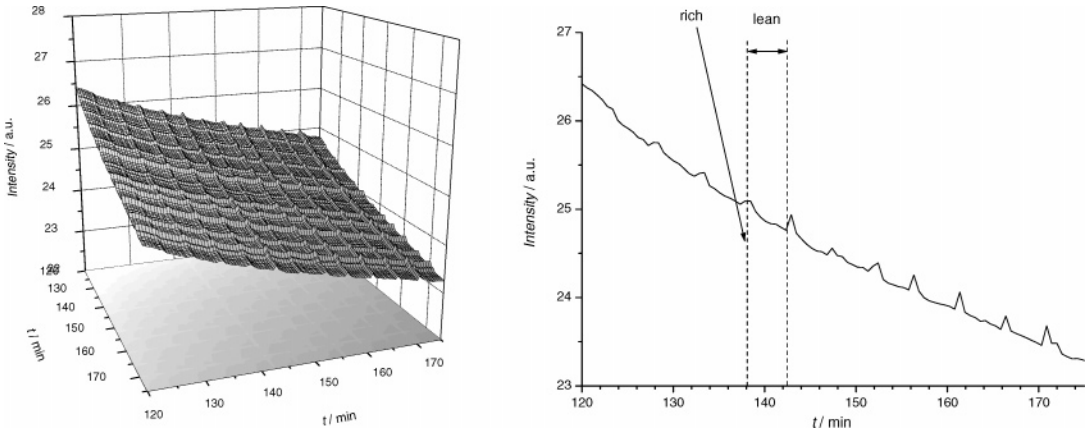

Figure 7. 2D sample−sample correlation analysis of the vibrations attributed to carbonates (1650−1350 cm^{-1}) at $\Delta t = 55$ min recorded while applying lean−rich cycling conditions. The surface plot is depicted on the left; the corresponding diagonal is depicted on the right.

trum recorded under rich conditions. The position of the bands obtained from the synchronous plot is depicted in Table 3. The cross-peak at the intersection Φ(1158 cm^{-1}, 1350−1290 cm^{-1}) is negative, indicating that the IR bands in the region 1350−1290 cm^{-1} decrease, while the IR band at 1158 cm^{-1} increases. The IR band located at 1442 cm^{-1} increases under rich operation conditions as indicated by a positive cross-peak appearing at the intersection 1160−1442 cm^{-1}. However, taking into consideration the experiments in absence of SO_2 (see Figure 3), it is assumed that this variation is caused by the reduction of sorbed NO_x species during the rich mode. The replacement of carbonates even under rich conditions is evidenced by the two negative cross-peaks (1557 cm^{-1}, 1158 cm^{-1}, and 1557 cm^{-1}, 1045 cm^{-1}), indicating a change in the opposite direction compared to the sulfate peaks centered at 1158 and 1045 cm^{-1}.

To confirm the results obtained for a single cycle, the calculations (2D moving window correlation analysis with a selection of five spectra) were performed on each of the 20 cycles showing similar results (not shown here). The carbonate species located at 1557 cm^{-1} decreased continuously throughout the experiment. During lean operation mode, the bands assigned to sulfate (1247, 1158, and 1045 cm^{-1}) increased, whereas the band assigned to carbonates (1442 cm^{-1}) decreased. During the rich operation mode, the bands centered at 1158 and 1045 cm^{-1} (sulfates) remained almost at a constant level, while the two bands at 1350 and 1295 cm^{-1} decreased in rich operation mode. The increase of the spectral intensity at 1442 cm^{-1} possibly resulted from an interaction of the S-trapping material with the NO_x species formed.

2D Sample-Sample Correlation Analysis. To follow the concentration profiles of the identified spectral regions, we applied the 2D sample−sample correlation analysis. The regions were selected as follows: 1650−1350 cm^{-1} (assigned to carbonate species), 1350−1290 cm^{-1} (assigned to transient sulfate species), and 1290−1000 cm^{-1} (assigned to bulklike sulfate species). It is important to note that several authors assigned bands in the latter region to surface sulfate species.[39,45] However, by means of moving window 2D correlation analysis no further peaks were identified, indicating a similar time-resolved behavior. Consequently, these species are more likely bulklike than surface species because of their nonreducibility under rich conditions. The dataset utilized for the calculation consisted of spectra for $\Delta t = 55$ min recorded under cycling reaction conditions after the 120-min lean treatment. The spectra used here represent a snapshot of the whole dataset.

The 2D sample−sample correlation analysis calculated for the wavenumber range of 1650−1350 cm^{-1} is depicted in Figure 7 (left) as well as the trace along the diagonal in Figure 7 (right). The general decrease in the intensity with increasing exposure to the gas mixture indicates that the intensity of the peaks located at 1437 and 1557 cm^{-1} decreased continuously throughout the experiment. After switching to rich conditions, the bands increased slightly in intensity, leading to the characteristic spike pattern similar to the one depicted in Figure 3. We speculate that this is related to reversibly adsorbed NO_x species formed during the rich mode (see Figure 3).

The 3D surface plot shown in Figure 8 (left) results from the 2D sample−sample correlation analysis in the region of 1350−1290 cm^{-1}. The intensity in the surface plot at the time location $X,Y = 120$ min,120 min is much smaller than the intensity at the spectra $X,Y = 175$ min,175 min, indicating that the bands in this region increased with time on stream. The trace along the diagonal [see Figure 8 (right)] contains a very characteristic (saw-tooth-like) pattern obtained during the lean−rich cycling. This pattern is characteristic of the changes in concentration of transient species, which is strongly diminished under rich conditions and formed under lean conditions.

Figure 9 shows the contour plot as well as the trace along the diagonal for the analysis of the region from 1290 to 1000 cm^{-1} attributed to S−O vibrations. The intensity in the surface plot at the time location $X,Y = 120$ min,120 min is much smaller than the intensity at the spectra $X,Y = 175$ min,175 min, which indicates that the bands located in the 1290−1000 cm^{-1} region increased with time, resulting from the adsorption of SO_2 and the formation of sulfate species. However, the spike-type pattern observed resembles that of the NO_2 adsorption shown in Figure 9 (right).

Determination of the Spectra of the Pure Components. After the identification of the spectral regions as well as the time-resolved concentration behavior, factor analysis in combination with the MCR-ALS technique was used for the determination of the spectra of the pure components. First, the number of significant components (shown in Table 4) was determined by a statistical analysis of the eigenvalues calculated for the dataset depicted in Figure 4.

The first and second eigenvalues are clearly found to be physically meaningful eigenvalues because of their significantly larger value compared to the others. Also, the third eigenvalue is considered to be a significant eigenvalue being more than 1 order of magnitude larger than the fourth eigenvalue. Moreover, the real error (RE, referring to the real error in the residual dataset) obtained for the remaining spectra is still approximately 50% larger than the value obtained for the fourth eigenvalue. Moreover, the values obtained for the reduced eigenvalue ratio

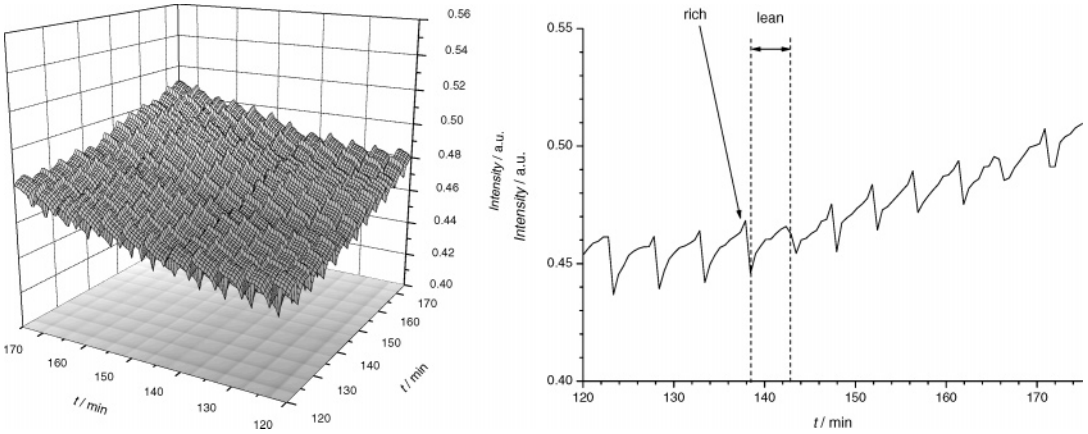

Figure 8. 2D sample−sample correlation analysis of the vibrations attributed to a transient species (1350−1290 cm^{-1}) at $\Delta t = 55$ min recorded while applying lean−rich cycling conditions. The surface plot is depicted on the left; the corresponding diagonal is depicted on the right.

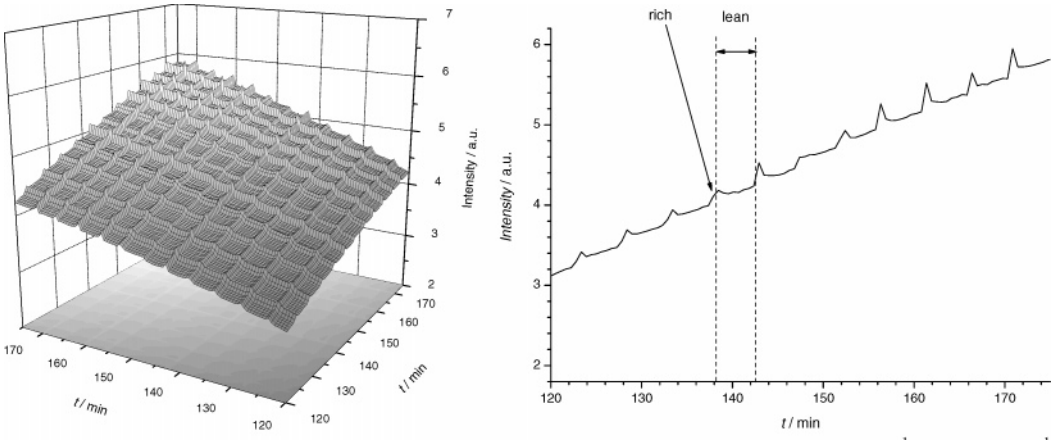

Figure 9. 2D sample−sample correlation analysis of the 1290−1000 cm^{-1} region at $\Delta t = 55$ min while applying lean−rich cycling conditions. The surface plot is depicted on the left; the corresponding diagonal is depicted on the right.

TABLE 4: Analysis of Eigenvalues Calculated Fort the Spectra Depicted in Figure 4

no.	EV	variance	REV	REVR	F-test	RE
1	7117.905	0.999938	0.26331	16064.38	240428.5	2.53E−05
2	0.4283	0.00006	1.64E−05	41.9264	593.3299	4.02E−06
3	0.00986	1.39E−06	3.91E−07	34.3226	284.9148	8.96E−07
4	2.77E−04	3.89E−08	1.14E−08	6.1338	18.3208	6.04E−07
5	4.35E−05	6.11E−09	1.86E−09	1.2398	3.5326	5.55E−07
6	3.38E−05	4.74E−09	1.50E−09	1.3083	3.3502	5.12E−07
7	2.48E−05	3.48E−09	1.14E−09	1.2511	2.9481	4.78E−07
8	1.90E−05	2.67E−09	9.15E−10	1.5165	2.675	4.48E−07
9	1.20E−05	1.68E−09	6.03E−10	1.2552	1.8969	4.33E−07
10	9.13E−06	1.28E−09	4.81E−10	1.1096	1.5893	4.22E−07

(REVR = 34.3226) and the F-test (284.9148) clearly indicate that the third eigenvalue can be attributed to physically relevant contributions in the spectra.

The statistical tests applied to the remaining eigenvalues showed a variance of more than 1 order of magnitude smaller than the third eigenvalue, indicating only a minor contribution to the meaningful dataset. Additionally, the RE differs only of ∼10% from the value obtained for the next eigenvalues, indicating that the fourth and all subsequent eigenvalues can be attributed to noise. Thus, the number of components in the present dataset is chosen to be three.

For the determination of physically meaningful information as mentioned in the Experimental Section, an initial coefficient matrix is necessary for the MCR-ALS technique. In the present contribution, the diagonals of the matrices obtained from the 2D sample−sample correlation analysis were used as the initial input for the coefficient matrix. Furthermore, nonnegativity constraints were applied to both coefficient and spectra matrix. The resulting spectra of the components and the coefficient matrix representing the time-resolved behavior of the pure components are depicted in Figure 10 and Figure 11, respectively.

The spectra of the three components are shown in Figure 10 and reveal clearly distinguishable peaks for every species. For the first species (A), they are located at 1557 and 1442 cm^{-1} are assigned to carbonate species, most likely $BaCO_3$.[13,37] The second species (B), show two distinct peaks at 1350 and 1295 cm^{-1}, which are located in the region typical for surface sulfate species, for example, on Al_2O_3.[47,48,50−52] Moreover, Waqif et al. assigned a band at 1350 cm^{-1} to a single S═O vibration resulting from a Al−(O_3)S═O species (at low sulfate coverage on Al_2O_3), whereas a second band at 1290 cm^{-1} appears at higher coverage.[53] This is in perfect agreement with the positions for the transient species identified here. The three peaks of the

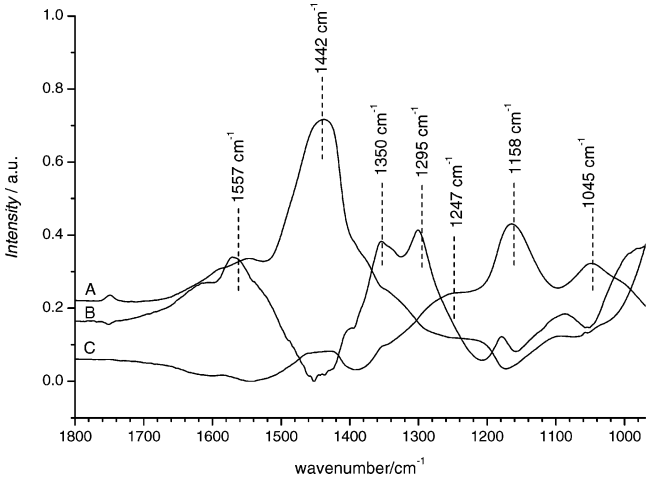

Figure 10. Spectra of the pure components (carbonates, A; surface sulfate species, B; bulk sulfate species, C) obtained from the spectra depicted in Figure 4 by means of MCR-ALS.

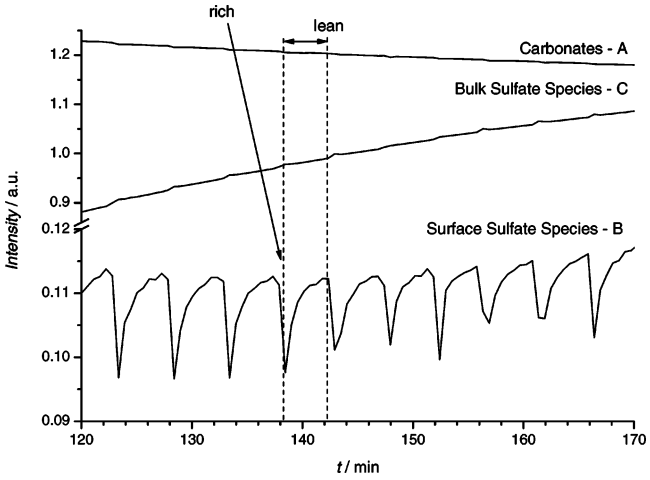

Figure 11. Coefficient matrix representing the concentration profile obtained from the spectra depicted in Figure 10 by means of MCR-ALS.

third species at 1247, 1158, and 1045 cm^{-1} (C) are located in the spectral region for SO stretching vibrations of uni- and bidentate sulfate species on a metal atom (Cu, Ba, or Al).[10,12,45,49,54−57] An unequivocal clear assignment is not possible because of the strongly overlapping regions of the single metal sulfates.

The corresponding coefficient matrix in Figure 11 (representing a time-resolved concentration profile) shows that carbonates (A) decreased in intensity, while sulfate species were formed. The transient surface sulfate species (B) shows a constant coverage. It is important to note that the spectra matrix was normalized. The carbonates (A) and the bulk sulfate species (C) contribution is about 9 times larger than the contribution of the saw-tooth-like species. Therefore, these bands were not readily observed in the 1D representation, while the application of the moving window 2D correlation analysis and MCR-ALS calculations allowed a clear identification.

Discussion

In situ XANES experiments at the S K-edge showed that sulfite species are formed under reaction conditions, which are reduced in the presence of Pt and could lead to the formation of SO_2 under rich conditions.[57] However, the impact of various sulfate-type species could not be distinguished because of the limitations of the XANES for assigning sulfur species of the same oxidation state.

The in situ IR spectroscopy experiments carried out under typical exhaust gas compositions at 523 K without SO_2 showed the formation of nitrates on the material, which were strongly affected by the changes between lean to rich reaction conditions (shown by the 2D sample−sample correlation analysis). The spike pattern observed under cycling conditions reveals the interaction of the sample with the C_3H_8 and the NO_x species adsorbed. Under rich conditions, this leads to an increase in the spectral intensity resulting potentially from the preferred formation of $C_3H_7-NO_2$ species, which is in good agreement with the findings for NSR catalysts during the reduction of the nitrates.[3,40] This pattern masks all experiments with NO_2 involved and, therefore, the spike is referred to the interaction with the NO_x species. It is important to note that in the region chosen for the 2D sample−sample correlation analysis carbonates and NO_x species appear. Therefore, a combination of two regimes that involve the reduction of the carbonate species and adsorption of NO_x species formed was observed leading to an overall decrease of the intensity.

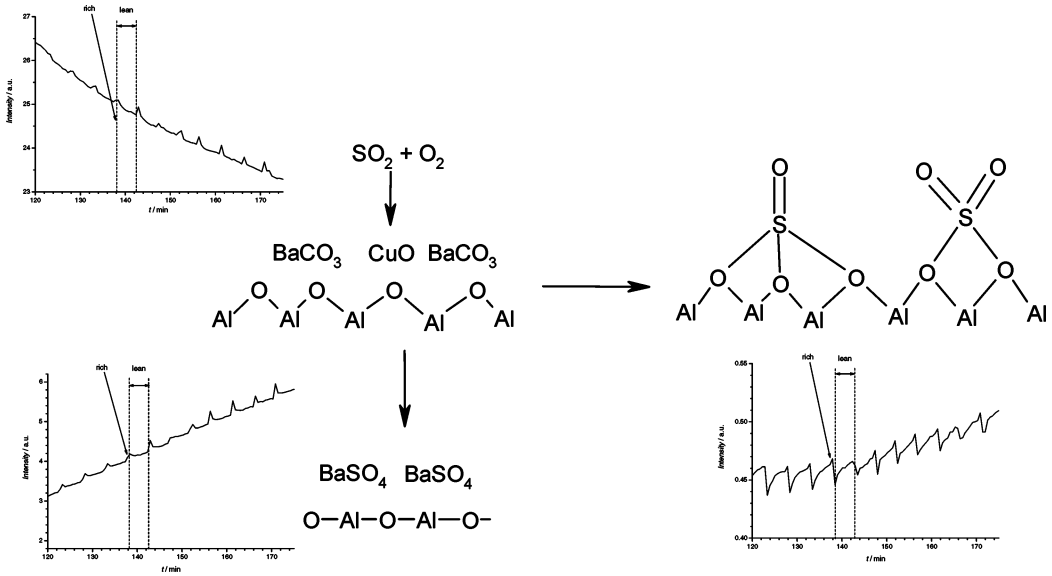

Figure 12. Species identified while the SO_x storage process under lean−rich cycling conditions on $Ba/CuO-Al_2O_3$.

Identification of the Sulfur Species. The extremely short time under rich conditions allowed the collection of only one spectrum under reducing conditions, representing a snapshot of the species formed. However, by applying the generalized 2D correlation analysis using the moving window approach individual spectral regions were clearly identified. The synchronous correlation plot indicates the formation of bulk and surface sulfate species under oxidizing conditions, which was accompanied by the simultaneous decomposition of the carbonate species.

In contrast, the synchronous correlation plot calculated from spectra recorded under lean and rich operation mode gives clear evidence for two new surface sulfate species on Al_2O_3 that appear at 1350 and 1295 cm^{-1}.[12,45] Surprisingly, the bands in the region for carbonates increased under rich conditions.

For the experiments carried out in absence of SO_2, this results from the interaction of the sample with the NO_x species formed under reducing conditions rather than formation of new carbonate species. This finding is supported by the decreasing intensities of other vibration modes of carbonate species during rich reaction conditions, which imply their removal.

Factor analysis gives a clear evidence for only three spectral contributions representing the whole dataset, which is in perfect agreement with the three spectral regions identified by means of 2D correlation analysis. A time-resolved quantitative description for all spectral regimes was possible by applying the 2D sample−sample correlation analysis. Only with these data, the application of the MCR-ALS technique (utilizing this as initial coefficient matrix) leads to the physically meaningful determination of the spectra of the pure components and their corresponding time-resolved coefficient profiles. The sulfur species identified on the material while the storage process are depicted in Figure 12. The bands in the carbonate region are identified as $BaCO_3$. The decreasing intensity suggests its decomposition, accompanied by an increasing (overall) intensity of the bulk sulfate species (conversion of carbonates to sulfates). The positions of the corresponding IR bands suggest the formation of bulk sulfate species on Ba and Cu rather than on Al_2O_3. The bands at 1350−1290 cm^{-1} suggest the formation of a sulfur species with a low surface coverage, presumably on Al_2O_3

The saw-tooth pattern implies a reduction of the concentration of the species under rich operation mode and a new formation of this under lean conditions. Therefore, the partial reduction of the species is concluded to lead to the release of SO_2, which has been observed in the plug flow SO_x uptake experiments (not shown here). The total contribution of the surface species on the surface is constant.

Conclusions

Transient surface sulfate species present under lean and rich fuel conditions applied on an industrial SO_2 sorbent were identified by applying advanced chemometric measures. With the combination of the generalized 2D correlation analysis, 2D sample−sample correlation analysis, and factor analysis using the MCR-ALS technique, the different regimes present on the sample were identified, separated, and characterized as functions of cycling conditions. A spike pattern in the concentration profiles was found to result from the interaction of NO_x species with the material. Three spectral regimes showing characteristic patterns for the SO_2 adsorption were identified: (i) carbonates decrease indicating their displacement by sulfates, (ii) bulk sulfates are generally increasing, and (iii) surface sulfate species showing a characteristic saw-tooth pattern. The clear identification and assignment of the adsorption site (Al_2O_3) of the surface sulfate species was carried out. The reduction of the surface sulfate species is related to a SO_2 release under rich conditions, which is an important step in the understanding of the SO_x storage process under lean−rich conditions.

Acknowledgment. This work was supported by the European Union in the framework of project G3RD-CT2002 00793.

References and Notes

(1) Matsumoto, S. I. *Catal. Today* **2004**, *90*, 183.
(2) Kreuzer, T.; Lox, E. S.; Lindner, D.; Leyrer, J. *Catal. Today* **1996**, *29*, 17.
(3) Sedlmair, C.; Seshan, K.; Jentys, A.; Lercher, J. A. *J. Catal.* **2003**, *214*, 308.
(4) Epling, W. S.; Campbell, L. E.; Yezerets, A.; Currier, N. W.; Parks, J. E. *Catal. Rev.—Sci. Eng.* **2004**, *46*, 163.
(5) Sedlmair, C.; Seshan, K.; Jentys, A.; Lercher, J. A. *Res. Chem. Intermed.* **2003**, *29*, 257.
(6) Limousy, L.; Mahzoul, H.; Brilhac, J. F.; Gilot, P.; Garin, F.; Maire, G. *Appl. Catal., B* **2003**, *42*, 237.
(7) Dathe, H.; Haider, P.; Jentys, A.; Fricke, R.; Schreier, H.; Lercher, J. A. *Phys. Chem. Chem. Phys.* **2006**, *13*, 1601.
(8) Dathe, H.; Peringer, E.; Roberts, V.; Jentys, A.; Lercher, J. A. *C. R. Chim.* **2005**, *8*, 753.
(9) Bailey, O. H.; Dou, D.; Molinier, M. *Soc. Automot. Eng., [Spec. Publ.] SP* **2000**, *SP-1533*, 257.
(10) Fang, H. L.; Wang, J. C.; Yu, R. C.; Wan, C. Z.; Howden, K. *Soc. Automot. Eng., [Spec. Publ.] SP* **2003**, *SP-1801*, 185.
(11) Waqif, M.; Saad, A. M.; Bensitel, M.; Bachelier, J.; Saur, O.; Lavalley, J. C. *J. Chem. Soc., Faraday Trans.* **1992**, *88*, 2931.
(12) Waqif, M.; Saur, O.; Lavalley, J. C.; Perathoner, S.; Centi, G. *J. Phys. Chem.* **1991**, *95*, 4051.
(13) Rohr, F.; Peter, S. D.; Lox, E.; Kogel, M.; Sassi, A.; Juste, L.; Rigaudeau, C.; Belot, G.; Gelin, P.; Primet, M. *Appl. Catal., B* **2005**, *56*, 201.
(14) Noda, I. *J. Am. Chem. Soc.* **1989**, *111*, 8116.
(15) Noda, I.; Dowrey, A. E.; Marcott, C. *Mikrochim. Acta* **1988**, *1*, 101.
(16) Noda, I. *Appl. Spectrosc.* **1993**, *47*, 1329.
(17) Noda, I.; Dowrey, A. E.; Marcott, C.; Story, G. M.; Ozaki, Y. *Appl. Spectrosc.* **2000**, *54*, 236A.
(18) Thibault-Starzyk, F.; Vimont, A.; Gilson, J. P. *Catal. Today* **2001**, *70*, 227.
(19) Sasic, S.; Muszynski, A.; Ozaki, Y. *J. Phys. Chem. A* **2000**, *104*, 6380.
(20) Sasic, S.; Muszynski, A.; Ozaki, Y. *J. Phys. Chem. A* **2000**, *104*, 6388.
(21) Keller, H. R.; Massart, D. L. *Chemom. Intell. Lab. Syst.* **1992**, *12*, 209.
(22) Thomas, M.; Richardson, H. H. *Vib. Spectrosc.* **2000**, *24*, 137.
(23) Jiang, J. H.; Ozaki, Y. *Appl. Spectrosc. Rev.* **2002**, *37*, 321.
(24) Jiang, T. H.; Liang, Y.; Ozaki, Y. *Chemom. Intell. Lab. Syst.* **2004**, *71*, 1.
(25) Malinowski, E. R. *Factor Analysis in Chemistry*, 3rd ed.; John Wiley & Sons Ltd.: New York, 2002.
(26) de Juan, A.; Tauler, R. *Anal. Chim. Acta* **2003**, *500*, 195.
(27) Tauler, R. d. J., A. MATLAB program MCR-ALS, MATLAB program EFA, http:/www.ub.es/gesq/eq1_eng.htm (accessed 02/16/2006), 2003.
(28) Mazet, V.; Carteret, C.; Brie, D.; Idier, J.; Humbert, B. *Chemom. Intell. Lab. Syst.* **2005**, *76*, 121.
(29) Noda, I. *Appl. Spectrosc.* **2000**, *54*, 994.
(30) Haider, P.; Chen, Y.; Lim, S.; Haller, G. L.; Pfefferle, L.; Ciuparu, D. *J. Am. Chem. Soc.* **2005**, *127*, 1906.
(31) Haider, P.; Haller, G. L.; Pfefferle, L.; Ciuparu, D. *Appl. Spectrosc.* **2005**, *59*, 1060.
(32) Gemperline, P. J. *J. Chem. Inf. Comput. Sci.* **1984**, *24*, 206.
(33) Fernandez-Garcia, M.; Alvarez, C. M.; Haller, G. L. *J. Phys. Chem.* **1995**, *99*, 12565.
(34) Marquez Alvarez, C.; Rodriguez Ramos, I.; Guerrero Ruiz, A.; Haller, G. L.; Fernandez Garcia, M. *J. Am. Chem. Soc.* **1997**, *119*, 2905.
(35) Karjalainen, E. J. *Chemom. Intell. Lab. Syst.* **1989**, *7*, 31.
(36) Tauler, R.; Casassas, E. *Chemom. Intell. Lab. Syst.* **1992**, *14*, 305.
(37) Miller, F. A.; Wilkins, C. H. *Anal. Chem.* **1952**, *24*, 1253.
(38) Aylor, A. W.; Larsen, S. C.; Reimer, J. A.; Bell, A. T. *J. Catal.* **1995**, *157*, 592.
(39) Nakamoto, K. *Infrared and Raman Spectra of Inorganic and Coordination Compounds*, 4th ed.; Wiley-Interscience: New York, 1986.
(40) Chi, Y. W.; Chuang, S. S. C. *J. Catal.* **2000**, *190*, 75.

(41) Hadjiivanov, K. I. *Catal. Rev.—Sci. Eng.* **2000**, *42*, 71.
(42) Westerberg, B.; Fridell, E. *J. Mol. Catal., A: Chem* **2001**, *165*, 249.
(43) Wan, Y.; Ma, J. X.; Wang, Z.; Zhou, W.; Kaliaguine, S. *Appl. Catal., B* **2005**, *59*, 235.
(44) Hayes, N. W.; Joyner, R. W.; Shpiro, E. S. *Appl. Catal., B* **1996**, *8*, 343.
(45) Yamaguchi, T. *Appl. Catal.* **1990**, *61*, 1.
(46) Iretskaya, S.; Mitchell, M. B. *J. Phys. Chem. B* **2003**, *107*, 4955.
(47) Babaeva, M. A.; Tsyganenko, A. A.; Filimonov, V. N. *Kinet. Catal.* **1985**, *25*, 787.
(48) Yao, H. C.; Stepien, H. K.; Gandhi, H. S. *J. Catal.* **1981**, *67*, 231.
(49) Sedlmair, C.; Seshan, K.; Jentys, A.; Lercher, J. A. *Catal. Today* **2002**, *75*, 413.
(50) Hubbard, C. P.; Otto, K.; Gandhi, H. S.; Ng, K. Y. S. *Catal. Lett.* **1995**, *30*, 41.
(51) Kijlstra, W. S.; Biervliet, M.; Poels, E. K.; Bliek, A. *Appl. Catal., B* **1998**, *16*, 327.
(52) Saur, O.; Bensitel, M.; Saad, A. B. M.; Lavalley, J. C.; Tripp, C. P.; Morrow, B. A. *J. Catal.* **1986**, *99*, 104.
(53) Waqif, M.; Saur, O.; Lavalley, J. C.; Wang, Y.; Morrow, B. A. *Appl. Catal.* **1991**, *71*, 319.
(54) Schoonheydt, R. A.; Lunsford, J. H. *J. Catal.* **1972**, *26*, 261.
(55) Centi, G.; Passarini, N.; Perathoner, S.; Riva, A. *Ind. Eng. Chem. Res.* **1992**, *31*, 1947.
(56) Decius, J. C.; Coker, E. H.; Brenna, G. L. *Spectrochim. Acta* **1963**, *19*, 1281.
(57) Hezel, A.; Ross, S. D. *Spectrochim. Acta* **1966**, *22*, 1949.
(58) Dathe, H.; Jentys, A.; Lercher, J. A. *J. Phys. Chem. B* **2005**, *109*, 21842.